



Interactive optimization of process parameters and coating analysis of laser cladding JG-3 powder

Ying Chen^{1,2} · Xin Wang³ · Yu Zhao^{1,2} · Boxue Song^{1,2} · Tianbiao Yu^{1,2}

Received: 29 July 2019 / Accepted: 2 March 2020 / Published online: 25 March 2020
© Springer-Verlag London Ltd., part of Springer Nature 2020

Abstract

As an advanced additive manufacturing technology, laser cladding has become a research hotspot in the fields of rapid manufacturing and surface modification in recent years. The quality of the cladding layer directly depends on the choice of process parameters. In order to obtain high quality cladding layer, the effects of laser power, scanning speed, and powder feeding rate on the quality of JG-3 iron-based powder cladding layer were studied by interaction orthogonal experiments. Three-dimensional measurement laser microscopy (3D MLM) and variance analysis were used to analyze the results. It was found that the interaction between laser power and powder feeding rate directly affects the optimum process parameters. Laser power 750 W, scanning speed 420 mm/min, and powder feeding rate 6.96 g/min were selected as the optimum process parameters. Scanning electron microscope (SEM), X-ray diffraction (XRD), and Thermo-Calc software were used to analyze the microstructure, phase composition, and solidification process of the coating, and compared with the experimental results. The results show that under the optimum process parameters, a dense crack-free and non-porous coating was obtained. The coating can be divided into three areas: coating zone (CZ), bonding zone (BZ), and heat affected zone (HAZ). The CZ is composed of α -Fe, Cr₂B, Fe₂B, and Cr₂₃C₆ phases. The calculated results obtained from the Thermo-Calc software are in good agreement with the experimental data. It is beneficial to the coating design for a desirable microstructure and mechanical properties.

Keywords Laser cladding · Interaction orthogonal test · Variance analysis · Process parameters · Microstructure · Thermo-Calc

✉ Tianbiao Yu
tianbiaoyudyx@gmail.com

Ying Chen
chenyingneu@gmail.com

Xin Wang
xinwang_research@163.com

Yu Zhao
zhaoyuneu@gmail.com

Boxue Song
1097451013@qq.com

- ¹ School of Mechanical Engineering and Automation, Northeastern University, Shenyang 110819, China
- ² Liaoning Provincial Key Laboratory of High-end Equipment Intelligent Design and Manufacturing Technology, Northeastern University, Shenyang 110819, China
- ³ The State Key Laboratory of Rolling and Automation, Northeastern University, Shenyang 110819, China

1 Introduction

Laser cladding is a rapid prototyping and surface modification technology, which has been developed in recent years [1, 2]. It has the characteristics of rapid condensation and rapid solidification, good metallurgical bonding between cladding layer and substrate, fine microstructure and high strength, and hardness [3, 4]. In order to obtain a better cladding layer and provide some theoretical basis for laser cladding powder, in recent years, many scholars or teams have studied the influence of process parameters on the macro morphology, microstructure, dilution rate, and mechanical properties of the cladding layer [5–10].

Goodarzi et al. [11] studied the effect of the process parameters on the coating geometry. The results show that laser power and scanning speed are the main parameters controlling the layer width. Marzban et al. [12] studied the effects of laser power, scanning speed, and powder feeding rate on the width, melting height, and depth of the cladding layer through L9

orthogonal experiment. Principal component analysis (PCA) and TOPSIS were combined to optimize the laser cladding process. The experimental results show that this method can effectively obtain the best combination of laser cladding parameters (laser power, 1 kw; scanning speed, 0.5 m/min; powder feeding rate, 8 mg/min.) Shi et al. [13] investigated and studied the parameter optimization and performance of 20CrMnTi low-carbon alloy steel composite powder. Taguchi OA and Topsis methods were used to optimize the process parameters of laser cladding gradient materials. Chen [14] used the orthogonal experimental design method to study the influence of laser additive manufacturing process on the characteristics of shaped parts. It was found that process parameters had the following influences on sedimentation characteristics: $W = -1.2206 + 0.0051P + 0.691D$, and $H = 10.2167 - 0.0075V + 0.7816R$. Laser power and spot diameter have important influence on cladding width, scanning speed, and powder feeding rate have significant influence on the cladding height.

In laser cladding, the microstructure and properties of coating specimens are dependent on the process parameters used. Marek et al. [15] analyzed the influence of process parameters on microstructure and abrasive wear resistance of laser clad WC-NiCrBSi coatings. It was found that the selection of process parameters is crucial, as they significantly affect the final coatings' wear resistance. In the cladding regions, the non-homogeneity of the coating's microstructure was responsible for significant selective abrasive wear behavior. Yu et al. [16] studied process parameter optimization and performance testing in direct laser manufacturing, and discussed in detail key parameters affecting part performance and process stability.

The above results show that in the laser cladding process, the process parameters have an important impact on the geometry and microstructure of the cladding layer, but the interaction of various factors in the laser cladding process is not considered, and the microstructure and phase of the cladding layer are not calculated in advance.

Iron-based alloy is a kind of alloy powder with low price, wide source, and good comprehensive performance. Widely used in many fields such as aerospace, industry, agriculture, and chemical industry. In this paper, JG-3 self-fluxing iron-based alloy powder is selected as the research object, and JIS S45C steel is used as the substrate. The effects of the main process parameters and their interactions on the microstructure and morphology of the cladding layer were studied to obtain a laser cladding layer with great morphology and uniform microstructure. The phase composition and

solidification process of the best coating were calculated by thermal calculation software, and the results were compared with experimental results. It provides some theoretical basis and technical support for part repair and cladding forming parts.

2 Experiment condition

2.1 Experimental materials

In this experiment, JIS S45C steel with the size of 120 mm × 100 mm × 10 mm³ was selected as the substrate. Polish the steel surface with sandpaper to remove the oxide film from the surface of the steel, and then clean with alcohol and dry. Cladding material is iron-based self-fluxing alloy powder JG-3 whose shape is nearly sphere. The powder is dried in a drying oven at a constant temperature of 80 °C for 6 h to prevent the powder from blocking the powder feeding pipe. The chemical composition of JG-3 powder and substrate material is shown in Table 1.

The powder size is selected between 100 and 400 screen mesh (38 μm–150 μm) and powder morphology is observed by scanning electronic microscope (SEM), as shown in Fig. 1.

2.2 Experimental facilities

The experiments were carried out on an open-loop laser cladding system, which includes a YLR-1000 optical fiber laser, a MCWL-50DTR water cooling machine, a RC52 cladding head, a vertical machining center, a double-cylinder powder feeder, an electrical control system, a laser operation integration cabinet, and a RC-CAM rapid prototyping software. The laser is continuous wave optical fiber; with a calibration wavelength of 1020 nm. The spot diameter is 2 mm, and the defocusing amount is 16 mm. The stability of the system is sufficient to meet the requirements of the DLF process. The working principle is shown in Fig. 2.

3 Experimental design

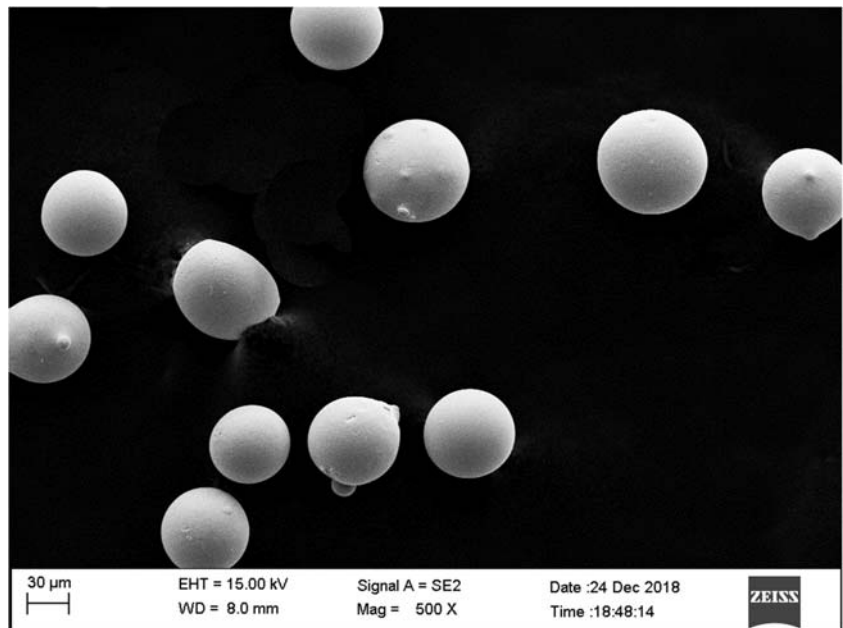
3.1 Factors and levels

In the practical work, there is more than one factor to measure the experimental results. In the multifactor orthogonal test, the quality or degree of one factor level is restricted by another

Table 1 Chemical composition (wt%) of JG-3 powder and substrate material(provided by the suppliers)

	C	Cr	Si	Ni	Mn	P,S	Cu	B	Fe
JG-3	0.12	16.5	0.8	–	–	–	–	0.9	Bal.
JIS S45C	0.42–0.5	≤0.25	0.17–0.37	≤0.25	0.5–0.8	≤0.045	≤0.25	–	Bal.

Fig. 1 The morphology of the powder JG-3



factor level, and there may be a certain contradictions between the optimal test schemes of each factor. Therefore, when analyzing the test results, we must comprehensively consider all factors and their interactions to find the best experimental scheme.

In the process of laser cladding, the geometry of cladding layer is highly affected by process parameters. In this paper, the orthogonal experimental method was used to study the influence of main process parameters (laser power, scanning speed, and powder feeding rate) and their

interaction on the quality of laser cladding JG-3 powder. According to the facilities and conditions of the laboratory, combined with the single-track single-factor experiments at the previous stage, the level value is determined by floating up and down at the best level. In order to facilitate the interaction analysis, each group of factors only takes 2 levels, and orthogonal scheme is designed to obtain the optimum process parameters of laser cladding JG-3 alloy. Specific experimental factors and levels are shown in Table 2.

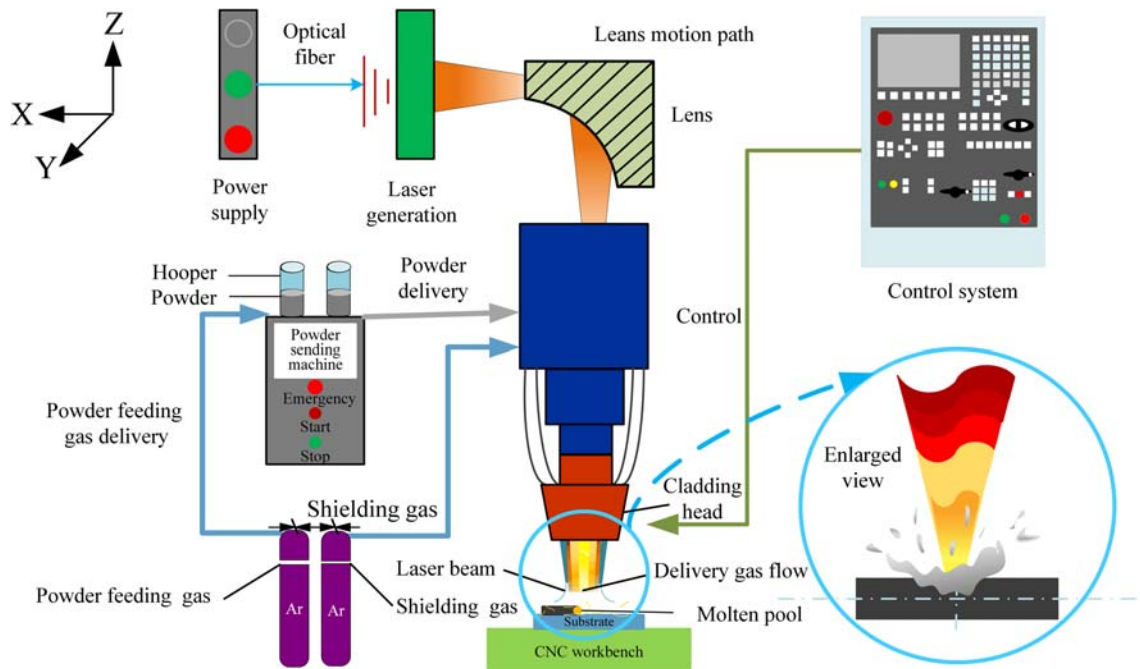


Fig. 2 Schematic of laser cladding process

Table 2 Factors and level of experiments

Level	Laser power (A)/W	Scanning speed (B)/(mm min ⁻¹)	Powder feeding rate (C)/(g min ⁻¹)
1	600	300	6.96
2	750	420	8.66

3.2 Interactive optimization scheme design

The key of interactive experimental scheme is the design of the Table head. The columns occupied by factors and interactions should be arranged correctly, otherwise, factors and interactions will be mixed together, and no clear and reliable results can be obtained [17].

Since this is a three-factor and two-level interaction orthogonal experiment, the sum of the degrees of freedom is $6(f_T = f_A + f_B + f_C + f_{A \times B} + f_{A \times C} + f_{B \times C} = 6)$, the number of experiments: $n \geq f_T + 1 = 7$. Therefore, the orthogonal table of $L_8(2^7)$ for 8 experiments was selected to arrange 3 factors A, B, and C, and the interaction between $A \times B$, $A \times C$, and $B \times C$ was considered. Table of $L_8(2^7)$ was shown in Table 3.

Arrange A and B as the first and second columns, respectively, and determine the position of interaction item $A \times B$ according to Table 3. First, find the column numbers (1) and (2) on the diagonal of the table, then look horizontally from (1) to the right, and look vertically from (2). The intersection is the number 3, that is, 3 is the column number of interaction item $A \times B$. Similarly, if factor C is arranged in the fourth column, the interaction terms $A \times C$ and $B \times C$ should be arranged in the fifth and sixth columns, respectively, and the seventh column should be arranged as the error column. Table head design is shown in Table 4, and the specific experimental scheme is shown in Table 5.

The quality of cladding layer formed by different process parameters has obvious difference. The improper selection of process parameters will lead to the failure of cladding layer and the formation of powder adhesion, porosity, and crack [18, 19]. In order to solve the above problems, according to the experimental design scheme, an interactive orthogonal experiment was established, and the results were analyzed.

Table 3 $L_8(2^7)$ interaction between two columns

Number	1	2	3	4	5	6	7
(1)	(1)	3	2	5	4	7	6
(2)		(2)	1	6	7	4	5
(3)			(3)	7	6	5	4
(4)				(4)	1	2	3
(5)					(5)	3	2
(6)						(6)	1
(7)							(7)

4 Results and discussion

4.1 Morphology analysis of cladding layer

The single-track experiment of laser cladding was performed on the substrate. The length of each track is about 26 mm, and the distance between them is 4.0 mm. Figure 3 shows the macro morphology of the sample surface. The surface of the coating is smooth without cracks and serious powder adhesion, which prove that the cladding powder has excellent processing performance.

The samples were cut perpendicular to the direction of the coatings with a wire cutting machine, then they were sanded with 240#, 400#, 600#, 800#, 1000#, 1500#, and 2000# sandpaper in sequence and polished with a water-grinding polishing paste having a particle size of 2.5. The samples were corroded by aqua regia, and then the morphology of samples was measured by three-dimensional measurement laser microscopy (3D MLM). The cross-section of single-track is shown in Fig. 4.

In order to optimize the process parameters of laser cladding JG-3 alloy powder, the depth, width, and height of the coatings were mainly measured, and the test results and computational analysis were listed in Table 6.

According to the test results shown in Table 6, the variance analysis method was used to analyze the effects of laser power, scanning speed, and powder feeding rate and the interaction between the two on the depth, width, and height of the coating.

F is the proportion of MS_j to MS_e. MS_j is the mean of the deviation squared sum of various factors, and MS_e is the mean of the deviation squared sum of errors. The F value reflects the importance of various factors on the target value. F value calculation method:

$$F_j = \frac{MS_j}{MS_e} \tag{1}$$

$$F_{ij} = \frac{MS_{ij}}{MS_e} \tag{2}$$

Table 4 Table head design

Factor	A	B	$A \times B$	C	$A \times C$	$B \times C$	Blank
Number	1	2	3	4	5	6	7

Table 5 Specific experimental scheme

No.	Laser cladding (A)/W	Scanning speed (B)/(mm min ⁻¹)	A × B	Powder feeding Rate(C)/(r min ⁻¹)	A × C	B × C	Error	Result
1	1	1	1	1	1	1	1	
2	1	1	1	2	2	2	2	
3	1	2	2	1	1	2	2	
4	1	2	2	2	2	1	1	
5	2	1	2	1	2	2	2	
6	2	1	2	2	1	1	1	
7	2	2	1	1	2	1	1	
8	2	2	1	2	1	2	2	

Among them, MS_e is the sum of the deviations squared of the error columns. Since the interaction only occupies 1 column, $MS_{ij} = MS_i$, the specific calculation method is as follows:

$$SS_j = \frac{1}{n} (K_1 - K_2)^2 \tag{3}$$

$$df_j = r - 1 \tag{4}$$

$$MS_j = \frac{SS_j}{df_j} \tag{5}$$

SS_j represents the sum of deviations squared of any column (j^{th} column) in the orthogonal table. The df_j and df_{ij} represent the degrees of freedom corresponding to any column of the orthogonal table and the degrees of freedom corresponding to the interaction column, respectively. The variance analysis is shown in Table 7.

It can be seen from Table 7, the effect of laser power on depth and width is very significant. Because the greater the laser power, the more laser is received by the powder and the substrate, the more energy is received, the more the powder melts, and the depth and width of the single-track clad increase.

The influence of scanning speed on height, width, and depth is sequentially reduced. The powder feeding rate has a significant effect on the height, and has a certain influence on

the depth and the width. In addition, the interaction between laser power and powder feeding rate has a certain influence on the height. It is necessary to consider the horizontal matching table of factors A and C, as shown in Table 8. Optimum schemes with the maximum width, the minimum depth and height are shown in Table 9.

If the influence of the interaction between A and C is not considered, the optimum solution is $A_1B_2C_2$. Considering the interaction, optimum solution is $A_2B_2C_1$, and it can be seen that the interaction have a direct impact on the selection of the optimum process parameters.

4.2 Dilution rate

Dilution rate plays an important role in the laser cladding process. First, it can ensure the bonding strength between the melt layers, form a high-quality metallurgical bond between the layers, and reduce internal defects (pore, crack, etc.); Moreover, it determines the remelting depth of the solidified melt layer, and directly affects the forming efficiency, the quality of the layer, and the stability of the coating [20–22]. The dilution rate η examines the percentage of the substrate material in the cladding area.

Since the true dilution range of the cladding area is mainly below the surface of the substrate, the dilution rate is usually calculated using the ratio of the cross-sectional area measurements. Figure 5 is a cross section diagram of laser cladding.

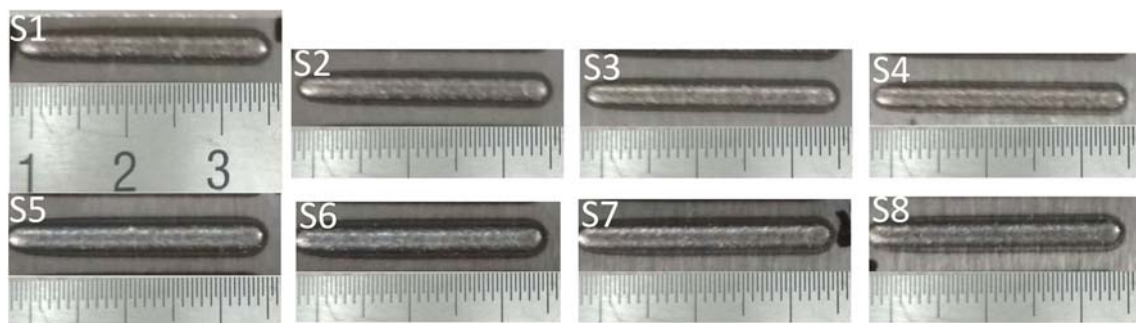


Fig. 3 Macro morphology of the coatings

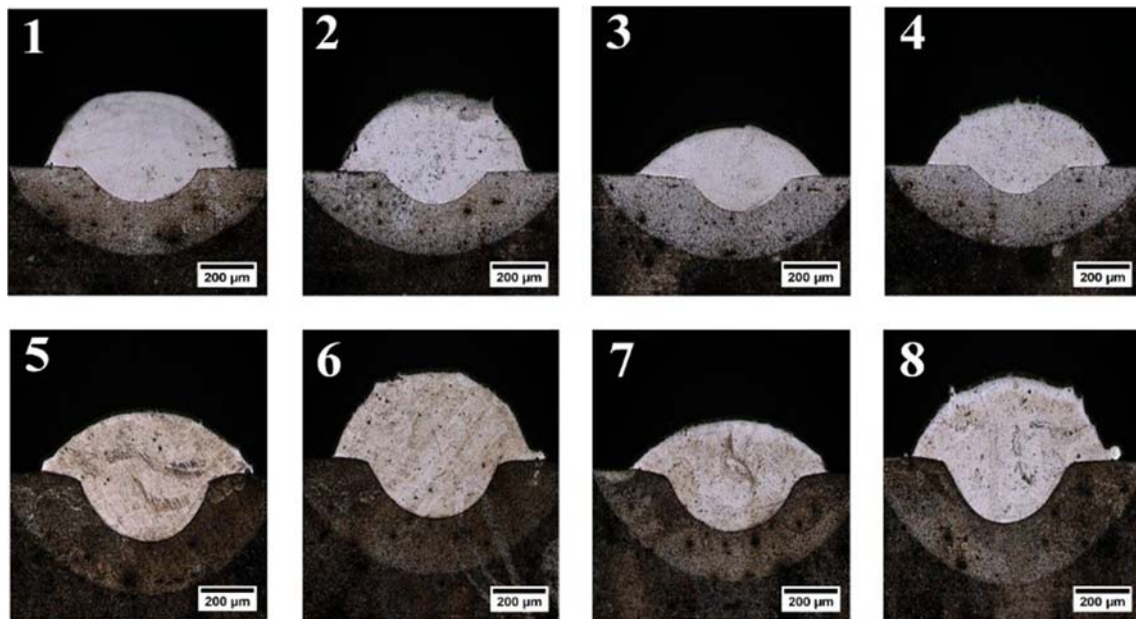


Fig. 4 Section morphology of single-track cladding layer

The formula for the dilution rate is $s = 2ab/3$, and the simplified one is the Formula (6) where w , h , and d are the width, height, and depth of the cladding area, respectively. Therefore,

the optimum process parameters affecting the dilution ratio of the cladding region can be found by paying attention to the height of the cladding region and the depth of the fusion zone.

Table 6 Test results and computational analysis

No.		A	B	AB	C	AC	BC	Blank	Depth (d)	Width (w)	Height (h)
1		1	1	1	1	1	1	1	301.5	1972.1	688.7
2		1	1	1	2	2	2	2	326.7	1982.1	718.7
3		1	2	2	1	1	2	2	301.5	1916.9	457.3
4		1	2	2	2	2	1	1	261.3	1881.9	542.8
5		2	1	2	1	2	1	2	618.2	2157.9	598.1
6		2	1	2	2	1	2	1	547.8	2062.7	824.2
7		2	2	1	1	2	2	1	557.9	2027.6	487.6
8		2	2	1	2	1	1	2	492.5	1987.3	648.3
Depth	K_1	1191	1794.2	1678.6	1779.1	1643.3	1673.5	1668.5	$T = 3407.4$		
	K_2	2216.4	1613.2	1728.8	1628.3	1764.1	1733.9	1738.9	$P = 1,451,296.845$		
	R	1025.4	181	50.2	150.8	120.8	60.4	70.4	$Q = 1,592,879.82$		
Factor importance		$C > B > A$									
Optimum schemes		$C_2B_2A_1$									
Width	K_1	7753	8174.8	7969.1	8074.5	7939	7999.2	7944.3	$T = 15,988.5$		
	K_2	8235.5	7813.7	8019.4	7914	8049.5	7989.3	8044.2	$P = 31,954,016.53$		
	R	482.5	361.1	50.3	160.5	110.5	9.9	99.9	$Q = 32,005,738.79$		
Factor importance		$A > B > C$									
Optimum schemes		$A_2B_1C_1$									
Height	K_1	2407.5	2829.7	2543.3	2231.7	2618.5	2477.9	2543.3	$T = 4965.7$		
	K_2	2558.2	2136	2422.4	2734	2347.2	2487.8	2422.4	$P = 3,082,272.061$		
	R	150.7	693.7	120.9	502.3	271.3	9.9	120.9	$Q = 3,189,668.41$		
Factor importance		$A > C > B$									
Optimum schemes		$A_1C_1B_2$									

Table 7 Variance analysis

Source of difference	SS	df	MS	F	Significance
Depth	A	131,431	1	131,431	283.55 *
	B	4095	1	4095	8.83 ⊖
	C	2843	1	2843	6.13 ⊖
	AC	1824	1	1824	3.94 ⊗
	AB	err	3	464	
	BC				
	e				
Total	10,152				
Width	A	29,101	1	29,101	55.39 *
	B	16,299	1	16,299	31.03 ⊗
	C	3220	1	3220	6.13 ⊖
	AC	1526	1	1526	2.91 ⊗
	AB	err	3	525	
	BC				
	e				
Total	22,621				
Height	A	2839	1	2839	3.09 ⊗
	B	60,152	1	60,152	65.41 *
	AB	1827	1	1827	1.99 ⊗
	C	31,538	1	31,538	34.29 *
	AC	9200	1	9200	10.00 ⊖
	BC	err	2	920	
	e				
Total	102,730				

* = significant impact; ⊗ = high impact; ⊖ = some impact; ⊗ = no significant impact

$$\eta = \frac{s_2}{s_1 + s_2} = \frac{\frac{2}{3}wd}{\frac{2}{3} \times w(h + d)} = \frac{d}{h + d} \tag{6}$$

The dilution rate of optimum schemes A₁B₂C₂ and A₂B₂C₁ were calculated based on the above analysis, and the results were 0.32 and 0.53, respectively. According to the previous experimental experience of the laboratory and the characteristics of powder, substrate, and equipment, the dilution rate of 40–60% is more appropriate. Too low dilution ratio, such as 1, 2, 3, and 4 in Fig. 4, does not have good combination with the substrate, and is easy to curl and peel off; while 5, 6, and 8 in Fig. 4, there are too many powder in one-time cladding, which exceeds the range of laser energy cladding, and pores and

Table 8 Factors A and C level collocation table

Factor	A ₁	A ₂
C ₁	(688.7 + 457.3)/2 = 573	(598.1 + 487.6)/2 = 542.85
C ₂	(718.7 + 542.8)/2 = 630.75	(824.2 + 648.3)/2 = 736.25

Table 9 Different indicator optimum schemes

Index	Factor order	Optimum scheme
Depth	A > B = C	A ₂ B ₁ C ₁
Width	A > B > C	A ₁ B ₂ C ₂
Height	B > C > A	A ₂ B ₂ C ₁

cracks are easily generated. From the perspective of dilution rate, scheme A₂B₂C₁ is better.

4.3 Verification and analysis

The quality of the cladding layer is affected by both the macro morphology and the microstructure. Since there are two optimization schemes considering and ignoring the interaction between process parameters, it is necessary to further analyze and verify the cladding layer quality.

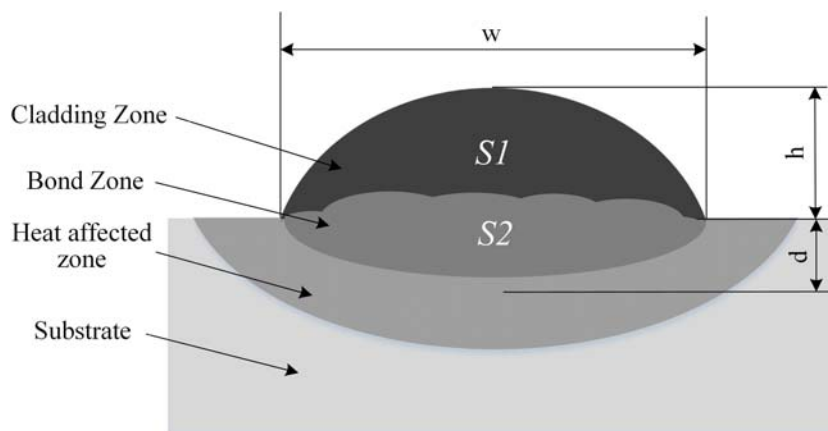
The microstructure of the optimized process parameter coating is shown in Fig. 6. It can be found that the entire cladding layer has no pores and cracks, and the cladding layer under the above optimized parameters has formed a good metallurgy combination with the substrate.

Figure 6a is the cross-section macrograph of a single-track coating, which can be divided into three regions: clad zone (CZ), bonding zone (BZ), and heat affected zone (HAZ). Figure 6b and c show the top and middle microstructure of the coating, respectively, which consist of equiaxed dendrites. Due to the high cooling rate of the top, it solidified when it has not yet nucleated to become bigger, and it is finer than the other parts, which plays an essential role in the wear resistance and hardness of the layer. In the middle of the cladding layer, uniform fine equiaxed dendrites with insignificant orientation are formed. Because the influence of the shielding gas is small, the distance from the substrate is far, the temperature gradient is not as large as that at the bottom, the heat dissipation loses its directivity, and the speed in all directions is basically the same, resulting in uniform equiaxed dendrites.

As shown in Fig. 6d, a columnar grain is generated at the bottom of the cladding layer, which is approximately perpendicular to the substrate. The reason is that the bottom of the cladding layer mainly relies on the heat dissipation of the substrate, and the temperature gradient is large, and the heat dissipation direction is perpendicular to the substrate, so the columnar grain is generated perpendicular to the substrate.

The microstructure of scheme A₁B₂C₂ cladding layer is shown in Fig. 7. There is not enough energy to melt the powder, and there is multiple powder adhesion on the outside of the cladding layer. And the molten pool formed is too small to dissipate heat before solidification, and finally, equiaxed grains appear instead of columnar crystals as shown in Fig. 6. At the top of the cladding layer and in the middle of the cladding layer are primary free dendrites and coarse

Fig. 5 Typical geometry characteristics of single-track cross-section



dendrites, respectively, rather than fine and uniform equiaxed dendrites, as shown in Fig. 7b and c. There is a region with poor metallurgical bonding between the cladding layer and the substrate. The molten metal liquid flows to the outermost layer of the molten pool, solidifies gradually during the flow process, and then forms an area that does not bond with the substrate, as shown in Fig. 7d, which is greatly detrimental to the formation quality. Therefore, in order to obtain better geometric morphology and forming quality, the optimized cladding scheme has obvious advantages over the scheme $A_1B_2C_2$.

The microstructure and X-ray diffraction spectrum of CZ under optimal process parameters are shown in Figs. 6 and 8. The microstructure of CZ is fine, uniform, and dense. The

phase constituents of the CZ are α -Fe, Cr_2B , Fe_2B , and $Cr_{23}C_6$ according to the index results of the X-ray diffraction spectrum as shown in Fig. 8.

It is necessary and interesting to analyze the solidification process, phase fractions, and phase compositions of laser clad Fe–base alloy coatings on JIS S45C steel. In Fig. 9, the temperature of the coating is on the transverse axis, and the molar fraction of the coating phase is on the longitudinal axis. So the relationship between phase fractions and temperature can be expressed from this figure. These lines represent the molar fraction of the phase calculated by Thermo-Calc software.

During laser cladding processing, laser beam irradiated the surface of the substrate, photon energy converted into heat, and propagated toward the interior. When the temperature is

Fig. 6 Micrographs of different zones in optimized cladding layer **a** morphology of single-track cross-section. **b** The top microstructure of the cladding layer. **c** The middle microstructure of the cladding layer. **d** The bottom microstructure of the cladding layer

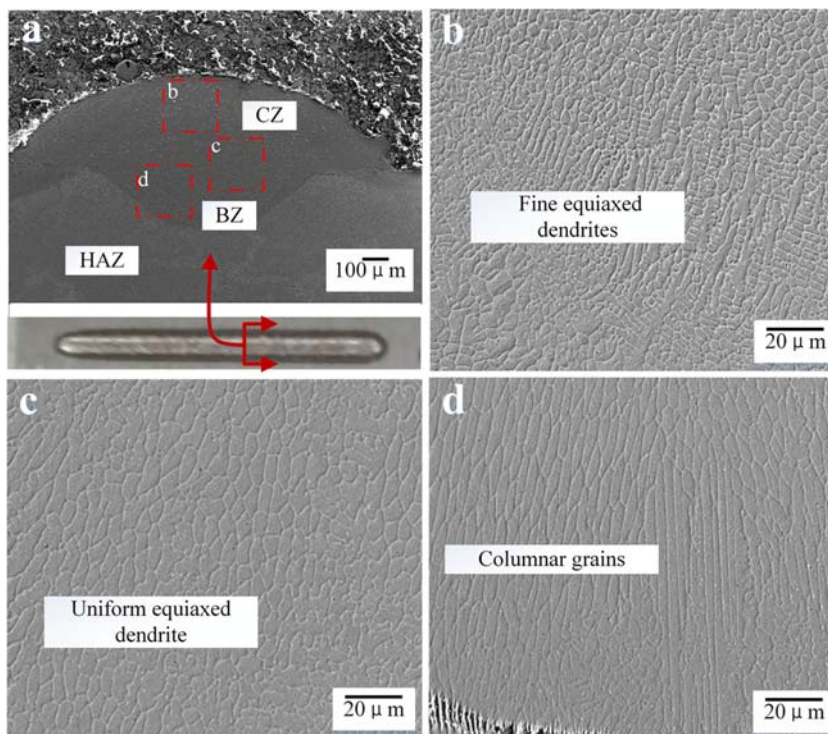
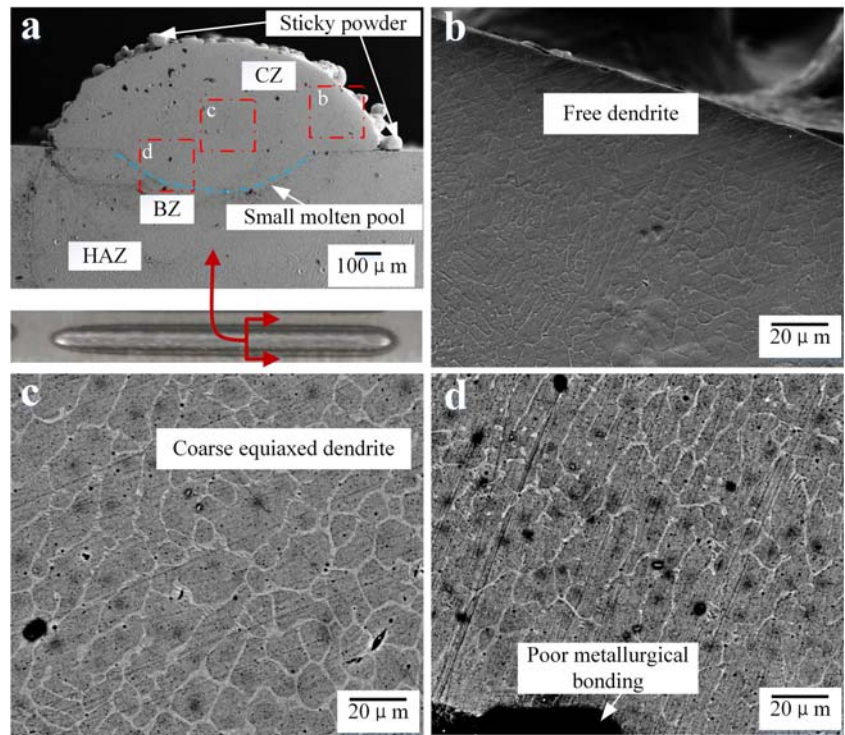


Fig. 7 Micrographs of different zones in under scheme $A_1B_2C_2$ **a** Morphology of single-track cross-section. **b** The top microstructure of the cladding layer. **c** The middle microstructure of the cladding layer. **d** The bottom microstructure of the cladding layer



higher than the melting point of the clad powder and the substrate, a molten pool is formed and part of the molten substrate comes into the coatings. And then the temperature of the molten pool decreases quickly due to the cooling down of the substrate. The solidification process and the reaction scheme in the coatings during the laser cladding process are as follows:

(1) Cr_2B and Fe_2B phases started to precipitate from the molten pool at about 1290 °C then quickly increased from zero to the maximal value 0.13 mol at about

1270 °C, while the amount of liquid phase reduced to zero when the temperature decreased to 1260 °C, as shown in Fig. 9.

- (2) As the temperature continuously decreased, the mole fraction of Cr_2B and Fe_2B phase remains unchanged still to 100 °C, whereas the fraction of austenite phase increased to the maximal value of 0.87 mol at about 1100 °C, and then remains unchanged to 900 °C.
- (3) The calculated mole fraction of $Cr_{23}C_6$ and ferrite phase almost firstly nucleated and grew up at the same

Fig. 8 X-ray diffraction spectrum of the clad specimen

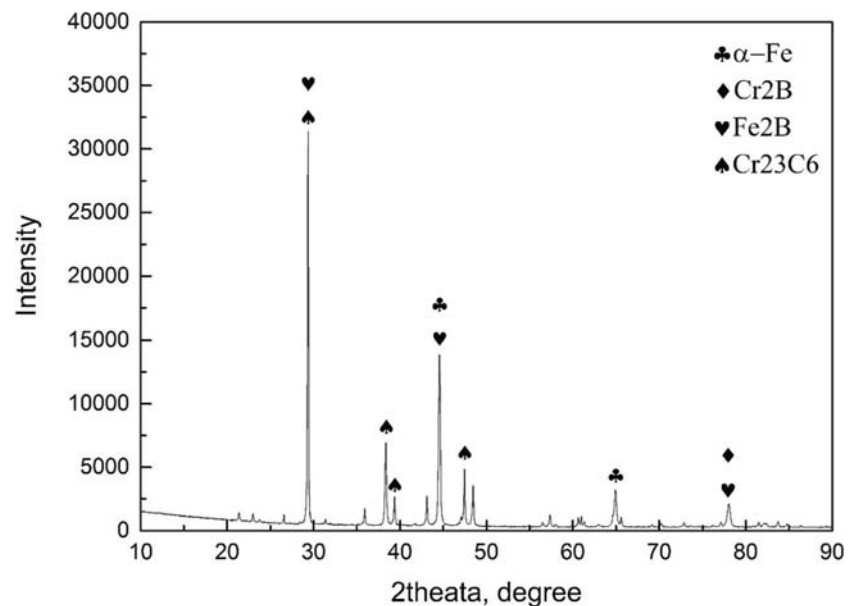
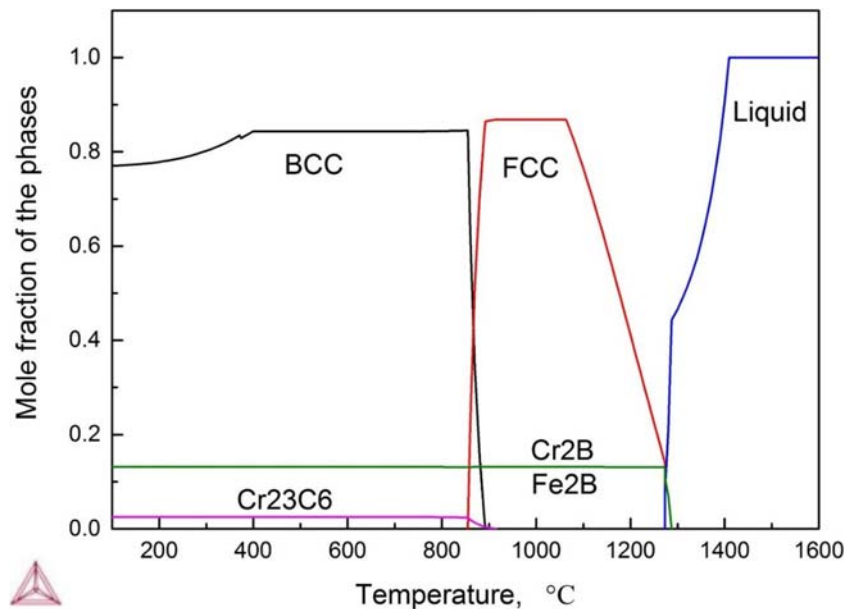


Fig. 9 Calculated phase fractions as a function of temperature for the coatings



temperature (900 °C), and the mole fraction of Cr_{23}C_6 and ferrite phase increased to 0.84 and 0.03 mol at 850 °C. Then Cr_{23}C_6 remained stable at 0.03, during which the ferrite remained stable at about 400 °C, and then gradually decreased to 0.77 mol.

According to the above analysis, the solidification process and reaction scheme of the molten pool during the laser cladding process are: $\text{Liquid} \rightarrow \text{Liquid} + \text{Cr}_2\text{B} + \text{Fe}_2\text{B} \rightarrow \text{Cr}_2\text{B} + \text{Fe}_2\text{B} + \text{austenite} \rightarrow \text{Cr}_2\text{B} + \text{Fe}_2\text{B} + \text{austenite} + \text{Cr}_{23}\text{C}_6 + \text{ferrite} \rightarrow \text{Cr}_2\text{B} + \text{Fe}_2\text{B} + \text{Cr}_{23}\text{C}_6 + \text{ferrite}$.

5 Conclusions

- (1) The interaction between laser power and powder feeding rate has a direct influence on the selection of the optimum process parameters. Considering this point, the optimum process parameters for laser cladding JG-3 powder are: laser power 750 W, scanning speed 420 mm/min, and powder feeding rate 6.96 g/min.
- (2) The experiment was carried out under optimum process parameters. Figure 6a is the transverse cross-section macrograph of the layer. The clad coatings are free from pores and cracks with a thickness of about 2.4 mm.
- (3) Through further microstructure comparative analysis, the optimized parameter combination is verified to ensure the reliability of the optimization results. The microstructure of the optimized process parameters is finer than that of other schemes, which have a positive effect on the hardness, wear resistance and other mechanical properties of the cladding layer.

- (4) The coating consists of three regions: CZ, BZ, and HAZ of the substrate. CZ consists of α -Fe, Cr_2B , Fe_2B , and Cr_{23}C_6 phases. The experimental results are in good agreement with the calculated results. It is beneficial to design coatings with a desirable microstructure and mechanical properties.

Funding information This work was supported by the National Ministry of Industry and Information Technology Green Manufacturing System Integration Funding Project [grant numbers 201675514], and Shenyang Science and Technology Plan Funding Project [grant number 18006001].

References

1. Lee H, Lim CHJ, Low MJ, Tham N, Murukeshan VM, Kim Y-J (2017) Lasers in additive manufacturing: a review. *Int J of Precis Eng and Manuf-Green Tech* 4(3):307–322. <https://doi.org/10.1007/s40684-017-0037-7>
2. Ahmed N (2019) Direct metal fabrication in rapid prototyping: a review. *J Manuf Process* 42:167–191. <https://doi.org/10.1016/j.jmapro.2019.05.001>
3. DebRoy T, Wei HL, Zuback JS, Mukherjee T, Elmer JW, Milewski JO, Beese AM, Wilson-Heid A, De A, Zhang W (2018) Additive manufacturing of metallic components process, structure and properties. *Prog Mater Sci* 92:112–224. <https://doi.org/10.1016/j.pmatsci.2017.10.001>
4. Enamian A, Alimardani M, Khajepour A (2014) Effect of cooling rate and laser process parameters on additive manufactured Fe–Ti–C metal matrix composites microstructure and carbide morphology. *J Manuf Process* 16(4):511–517. <https://doi.org/10.1016/j.jmapro.2014.07.002>
5. Shamsaei N, Yadollahi A, Bian L, Thompson SM (2015) An overview of direct laser deposition for additive manufacturing; part II: mechanical behavior, process parameter optimization and control. *Addit Manuf* 8:12–35. <https://doi.org/10.1016/j.addma.2015.07.002>

6. Cheng YH, Cui R, Wang HZ, Han ZT (2017) Effect of processing parameters of laser on microstructure and properties of cladding 42CrMo steel. *Int J Adv Manuf Technol* 96(5–8):1715–1724. <https://doi.org/10.1007/s00170-017-0920-y>
7. Zhu LD, Wang SH, Pan HC, Yuan CT, Chen XS (2020) Research on remanufacturing strategy for 45 steel gear using H13 steel powder based on laser cladding technology. *J Manuf Process* 49:344–354. <https://doi.org/10.1016/j.jmapro.2019.12.009>
8. Lei YW, Sun RL, Tang Y, Niu W (2015) Microstructure and phase transformations in laser clad Cr_xS_y/Ni coating on H13 steel. *Opt Lasers Eng* 66:181–186. <https://doi.org/10.1016/j.optlaseng.2014.09.006>
9. Li HN, Yang Y, Zhao YJ, Zhang Z, Zhu W, Wang W, Qi H (2019) On the periodicity of fixed-abrasive planetary lapping based on a generic model. *J Manuf Process* 44:271–287. <https://doi.org/10.1016/j.jmapro.2019.05.036>
10. Liu S, Kovacevic R (2014) Statistical analysis and optimization of processing parameters in high-power direct diode laser cladding. *Int J Adv Manuf Technol* 74(5–8):867–878. <https://doi.org/10.1007/s00170-014-6041-y>
11. Goodarzi DM, Pekkarinen J, Salminen A (2017) Analysis of laser cladding process parameter influence on the clad bead geometry. *Weld World* 61(5):883–891. <https://doi.org/10.1007/s40194-017-0495-0>
12. Marzban J, Ghaseminejad P, Ahmadzadeh MH, Teimouri R (2014) Experimental investigation and statistical optimization of laser surface cladding parameters. *Int J Adv Manuf Technol* 76(5–8):1163–1172. <https://doi.org/10.1007/s00170-014-6338-x>
13. Shi Y, Li Y, Liu J, Yuan Z (2018) Investigation on the parameter optimization and performance of laser cladding a gradient composite coating by a mixed powder of Co50 and Ni/WC on 20CrMnTi low carbon alloy steel. *Opt Laser Technol* 99:256–270. <https://doi.org/10.1016/j.optlastec.2017.09.010>
14. Chen B, Mazumder J (2017) Role of process parameters during additive manufacturing by direct metal deposition of Inconel 718. *Rapid Prototyp J* 23(5):919–929. <https://doi.org/10.1108/RPJ-05-2016-0071>
15. Vostřák M, Houdková Š, Bystrianský M, Česánek Z (2018) The influence of process parameters on structure and abrasive wear resistance of laser clad WC-NiCrBSi coatings. *Mater Res Express* 5(9):096522. <https://doi.org/10.1088/2053-1591/aad859>
16. Yu TB, Zhao Y, Sun JY, Chen Y, Qu WR (2018) Process parameters optimization and mechanical properties of forming parts by direct laser fabrication of YCF101 alloy. *J Mater Process Technol* 262:75–84. <https://doi.org/10.1016/j.jmatprotec.2018.06.023>
17. Younas M, Jaffery SHI, Khan M, Khan MA, Ahmad R, Mubashar A, Ali L (2019) Multi-objective optimization for sustainable turning Ti6Al4V alloy using grey relational analysis (GRA) based on analytic hierarchy process (AHP). *Int J Adv Manuf Technol* 105:1175–1188. <https://doi.org/10.1007/s00170-019-04299-5>
18. Goodarzi DM, Pekkarinen J, Salminen A (2015) Effect of process parameters in laser cladding on substrate melted areas and the substrate melted shape. *J Laser Appl* 27(S2):S29201. <https://doi.org/10.2351/1.4906376>
19. Guo P, Zou B, Huang C, Gao H (2017) Study on microstructure, mechanical properties and machinability of efficiently additive manufactured AISI 316L stainless steel by high-power direct laser deposition. *J Mater Process Technol* 240:12–22. <https://doi.org/10.1016/j.jmatprotec.2016.09.005>
20. Liu HM, Hu ZQ, Qin XP, Wang YL, Zhang J, Huang S (2017) Parameter optimization and experimental study of the sprocket repairing using laser cladding. *Int J Adv Manuf Technol* 91:3967–3975. <https://doi.org/10.1007/s00170-017-0066-y>
21. Campanelli SL, Angelastro A, Signorile CG, Casalino G (2017) Investigation on direct laser powder deposition of 18 Ni (300) marage steel using mathematical model and experimental characterisation. *Int J Adv Manuf Technol* 89:885–895. <https://doi.org/10.1007/s00170-016-9135-x>
22. Liu B, Liu HP, Jing XB, Li YX, Bai PK (2018) The effect of laser process parameters on microstructure and dilution rate of cladding coatings. *IOP Conf Ser Mater Sci Eng* 307:012035. <https://doi.org/10.1088/1757-899x/307/1/012035>

Publisher's note Springer Nature remains neutral with regard to jurisdictional claims in published maps and institutional affiliations.